Eur. Phys. J. C 35, 137–143 (2004)
Digital Object Identifier (DOI) 10.1140/epjc/s2004-01777-5

THE EUROPEAN PHYSICAL JOURNAL C

Testing non-commutative QED $\gamma\gamma\gamma$ and $\gamma\gamma\gamma\gamma$ couplings at LHC

S.M. Lietti[1,a], C.A. de S. Pires[2,b]

[1] Instituto de Física da USP, C.P. 66.318, São Paulo, SP 05389-970, Brazil
[2] Departamento de Física da UFPb, C.P. 5008, João Pessoa, PB 58051-970, Brazil

Received: 9 February 2004 / Revised version: 27 February 2004 /
Published online: 8 April 2004 –

Abstract. In this work, we investigate the sensitivity of the process $p + p \to q + q \to j + j + \gamma + \gamma$ at LHC for the photonic 3- and 4-point functions that appear in non-commutative QED. We show that this process serves to study the behavior of the space-space as well as of the space-time non-commutativity. We also show that this process can probe the non-commutative scale Λ in the range of a few TeV.

1 Introduction

The central idea behind non-commutative space-time (NCST) is that there must be a regime of energy where space-time loses its condition of continuum and starts to obey the relation $[\hat{x}_\mu, \hat{x}_\nu] = \mathrm{i}\frac{C_{\mu\nu}}{\Lambda^2}$ [1], where $C_{\mu\nu}$ is a real antisymmetric constant matrix. In other words, there must be a very microscopic region of space-time, or very high energy, where our common understanding of space-time is not applicable anymore.

When people began to develop such an idea, the scale of energy Λ where non-commutativity was expected to bcome manifest was around the Planck scale M_{Pl} [2, 3]. This scale of energy is quite out of the present phenomenological reach. However, inspired by this recent idea of extra dimensions [4], which suggest that the fundamental Planck scale can be around a few TeV, people brought Λ down to the TeV scale [5]. This leaves the idea of NCST phenomenologically attainable. In this regard, it may turn out to be interesting to reformulate the phenomenological models on the basis of the NCST.

Unfortunately, the implementation of NCST is still a challenge for model building and presently the only consensual phenomenological model is non-commutative QED (NCQED) [5–8]. The phenomenology of NCQED has been intensively investigated [5–8]. What has particularly called the people's attention in NCQED is the photonic 3- and 4-point functions. The processes where such couplings appear are the Compton scattering, pair annihilation process, $e^+e^- \to \gamma\gamma$, and $\gamma\gamma \to \gamma\ \gamma$.

However, no process involving quarks was investigated yet. The reason is that in NCQED, the covariant derivatives can only be constructed for fermionic fields of charges 0 and ± 1. Therefore, the non-commutative photon–quark–quark interaction cannot be described by the model. In order to solve this problem, people began to implement the NCST effects into the standard model of particles. Two proposals for non-commutative standard model (NCSM) can be found in the literature; one is based on the $U_\star(3) \times U_\star(2) \times U_\star(1)$ gauge group [9], while the other is based on the standard gauge group $SU(3)_C \times SU(2)_{\mathrm{L}} \times U(1)_Y$, making use of the Seiberg–Witten maps [10]. Some phenomenology of these models is found in [11]. However, no agreement has been reached yet regarding phenomenological NCSM.

Therefore, our main goal in this work is to study the potential of the LHC to only probe NCQED, particularly the photonic 3- and 4-point functions, $\gamma\gamma\gamma$ and $\gamma\gamma\gamma\gamma$, through the process $p + p \to q + q \to j + j + \gamma + \gamma$. In order to do so, the only assumption we made is that a possible non-commutative quark–quark–photon interaction generates negligible effects, allowing us to consider only the standard model quark–quark–photon interaction and NCQED in our analysis.

This work is organized as follows. In Sect. 2 we present the photonic 3- and 4-point functions in NCQED. Next in Sect. 3 we discuss the NCQED signal and the SM background. In Sect. 4, we finish with our conclusions.

2 Photonic 3- and 4-point functions in NCQED

One manner of settling non-commutative coordinates in the context of field theory is through the Moyal product, or the $\star$ product, whose expansion is [2]

$$A(x) \star B(x) \equiv [\mathrm{e}^{(\mathrm{i}/2)\theta_{\mu\nu}\partial_{\zeta\mu}\partial_{\eta\nu}} A(x+\zeta)B(x+\eta)]_{\zeta=\eta=0}. \quad (1)$$

With this product, we proceed in the following way. We first formulate the Lagrangian in terms of this $\star$ product and then change the $\star$ product by the expansion in (1) in order to leave the Lagrangian in terms of an ordinary product.

[a] e-mail: lietti@fma.if.usp.br
[b] e-mail: cpires@fisica.ufpb.br

In gauge theories the first thing to do is to express the gauge transformation in terms of the $\star$ products:

$$A_\mu \to U \star A_\mu \star U^{-1} + \frac{\mathrm{i}}{g} U \star \partial_\mu U^{-1}. \tag{2}$$

In the particular case of NCQED, where $U(x) = \exp\star(\mathrm{i}g\alpha(x))$, we have

$$A_\mu \to A_\mu + \partial_\mu \alpha - \mathrm{i}g(A_\mu \star \alpha - \alpha \star A_\mu). \tag{3}$$

In order for the action of the NCQED to preserve gauge invariance, the tensor $F^*_{\mu\nu}$ must lend itself to be presented in the form

$$\begin{aligned} F^*_{\mu\nu} &= \partial_\mu A_\nu - \partial_\nu A_\mu - \mathrm{i}g[A_\mu, A_\nu]_\star \\ &= F_{\mu\nu} - \mathrm{i}g(A_\mu \star A_\nu - A_\nu \star A_\mu). \end{aligned} \tag{4}$$

With these expansions, the photonic part of the NCQED presents the following Lagrangian:

$$\begin{aligned} \mathcal{L} = &-\frac{1}{4}F^{\mu\nu}F_{\mu\nu} - 2e\sin\left(\frac{p_1 C p_2}{2\Lambda^2}\right)(\partial_\mu A_\nu - \partial_\nu A_\mu)A^\mu A^\nu \\ &- 4e^2 \sin^2\left(\frac{p_1 C p_2}{2\Lambda^2}\right) A^4, \end{aligned} \tag{5}$$

where $p_1 C p_2 = p_1^\mu p_2^\nu C_{\mu\nu}$ and with $F_{\mu\nu} = \partial_\mu A_\nu - \partial_\nu A_\mu$ being the standard electromagnetic tensor. The Feynman rules for the vertices $\gamma\gamma\gamma$ and $\gamma\gamma\gamma\gamma$ are given by [5]

$$\begin{aligned} &\gamma_\mu(p_1)\gamma_\nu(p_2)\gamma_\rho(p_3): \\ &2g\sin\left(\frac{p_1 C p_2}{2\Lambda^2}\right) \\ &\times[(p_1-p_2)^\rho g^{\mu\nu} + (p_2-p_3)^\mu g^{\nu\rho} + (p_3-p_1)^\nu g^{\mu\rho}]\,; \\ &\gamma_\mu(p_1)\gamma_\nu(p_2)\gamma_\rho(p_3)\gamma_\sigma(p_4): \\ &4\mathrm{i}g^2\left[(g^{\mu\sigma}g^{\nu\rho} - g^{\mu\rho}g^{\nu\sigma})\sin\left(\frac{p_1 C p_2}{2\Lambda^2}\right)\sin\left(\frac{p_3 C p_4}{2\Lambda^2}\right)\right. \\ &\quad +(g^{\mu\rho}g^{\nu\sigma} - g^{\mu\nu}g^{\rho\sigma})\sin\left(\frac{p_3 C p_1}{2\Lambda^2}\right)\sin\left(\frac{p_2 C p_4}{2\Lambda^2}\right) \\ &\quad \left. +g^{\mu\nu}g^{\rho\sigma} - g^{\mu\sigma}g^{\nu\rho}()\sin\left(\frac{p_1 C p_4}{2\Lambda^2}\right)\sin\left(\frac{p_2 C p_3}{2\Lambda^2}\right)\right], \end{aligned} \tag{6}$$

where all the momenta are out-going.

The parameterization suggested by Hewett–Petriello–Rizzo [5] for the antisymmetric matrix C is

$$C_{\mu\nu} = \begin{pmatrix} 0 & \sin\alpha\cos\beta & \sin\alpha\sin\beta & \cos\alpha \\ -\sin\alpha\cos\beta & 0 & \cos\gamma & -\sin\gamma\sin\beta \\ -\sin\alpha\sin\beta & -\cos\gamma & 0 & -\sin\gamma\cos\beta \\ -\cos\alpha & \sin\gamma\sin\beta & \sin\gamma\cos\beta & 0 \end{pmatrix}, \tag{7}$$

where the three angles used to parameterize $C_{\mu\nu}$ are related with the direction of the background **E**- and **B**-fields. In this parameterization, the angle β defines the origin of the ϕ axis [5]. The common procedure here is to fix ϕ by setting $\beta = \pi/2$. Therefore, the antisymmetric matrix gets parameterized by two angles: the angle α related to the space-time non-commutativity, and the angle γ related to the space-space non-commutativity.

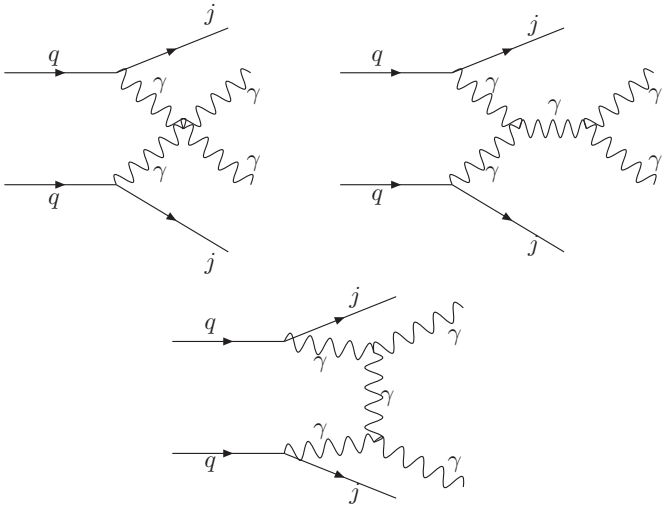

Fig. 1. NCQED photonic 3- and 4-point functions contributions for the reaction (8)

In order to test the NCQED vertexes given by (6), we perform a detailed analysis of the production via weak boson fusion (WBF) of photon pairs accompanied by jets, i.e.,

$$p + p \to q + q \to j + j + \gamma + \gamma\,. \tag{8}$$

Beyond the expected SM Feynman diagrams, the reaction (8) receives contributions from NCQED photonic 3- and 4-point functions, as shown in Fig. 1.

The advantage of WBF, where the scattered final-state quarks receive a significant transverse momentum and are observed in the detector as far-forward/backward jets, is the strong reduction of QCD backgrounds due to the kinematical configuration of the colored part of the event.

3 Signals and backgrounds

In this section we study the reaction (8) at the LHC. We evaluated numerically the helicity amplitudes of all the SM subprocesses leading to the $jj\gamma\gamma$ final state where j can be either a gluon, a quark or an anti-quark in our partonic Monte Carlo. The SM amplitudes were generated using Madgraph [12] in the framework of Helas [13] routines. The NCQED interactions arising from the Lagrangian (5) were implemented as subroutines and were included accordingly. We consistently took into account the effect of all interferences between the NCQED and the SM amplitudes, and considered a center-of-mass energy of 14 TeV and an integrated luminosity of $100\,\mathrm{fb}^{-1}$ for LHC.

The process (8) receives contributions from the NCQED $\gamma\gamma\gamma$ and $\gamma\gamma\gamma\gamma$ vertices. In order to reduce the enormous QCD background we must exploit the characteristics of the WBF reactions. The main feature of WBF processes

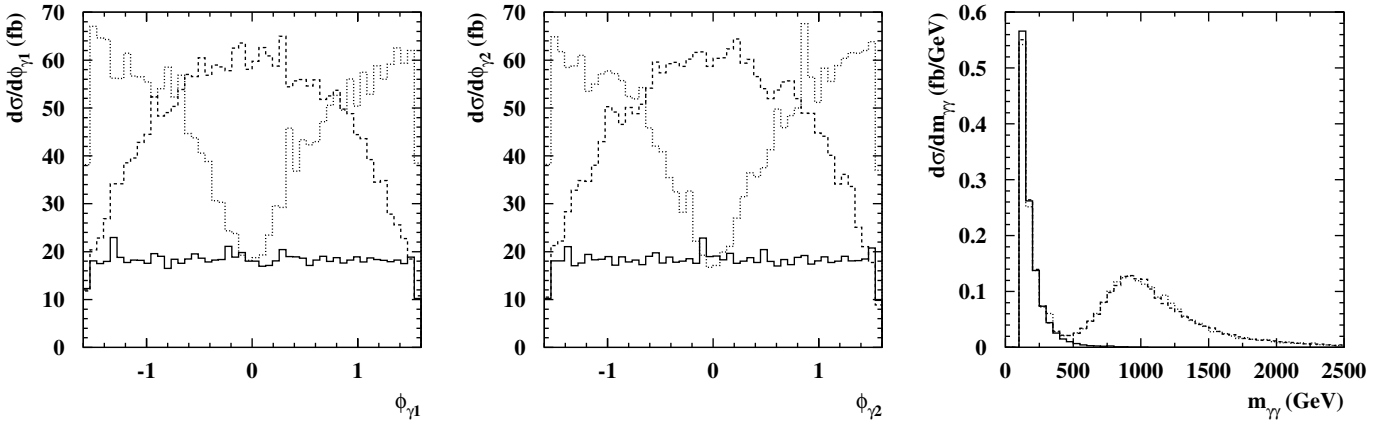

Fig. 2. Azimuthal angle distribution of the most energetic final photon ($\Phi_{\gamma 1}$), azimuthal angle distribution of the least energetic final photon ($\Phi_{\gamma 2}$), and invariant mass distribution of the $\gamma\gamma$ pair ($m_{\gamma\gamma}$) for the reaction $pp \to \gamma\gamma jj$. The full line represents the SM distribution. The NCQED contribution was obtained for $\Lambda = 250\,\mathrm{GeV}$, and the angles α, β and γ equal to $\pi/2$. The dashed (dotted) line represents the space-space (space-time) non-commutativity case, discussed in the text

is a pair of very far-forward/backward tagging jets with significant transverse momentum and large invariant mass between them. Therefore, we required that the jets should comply with[1]

$$\begin{aligned} & p_T^{j_{1(2)}} > 40\ (20)\,\mathrm{GeV}, \quad |\eta_{j_{(1,2)}}| < 5.0\ , \\ & |\eta_{j_1} - \eta_{j_2}| > 4.4, \quad \eta_{j_1} \cdot \eta_{j_2} < 0 \quad \text{and} \\ & \Delta R_{jj} > 0.7\ . \end{aligned} \tag{9}$$

Furthermore, the photons are central, typically being between the tagging jets. So, we require that the photons satisfy

$$\begin{aligned} & E_T^{\gamma_{(1,2)}} > 25\,\mathrm{GeV} \quad , \quad |\eta_{\gamma_{(1,2)}}| < 2.5\ , \\ & \min\{\eta_{j_1}, \eta_{j_2}\} + 0.7 < \eta_{\gamma_{(1,2)}} < \max\{\eta_{j_1}, \eta_{j_2}\} - 0.7\ , \\ & \Delta R_{j\gamma} > 0.7 \quad \text{and} \quad \Delta R_{\gamma\gamma} > 0.4\ . \end{aligned} \tag{10}$$

Several kinematic distributions were evaluated in order to reduce the SM background with minimum impact over the NCQED signal. Better results were observed in three distributions: the azimuthal angle distribution of the most energetic final photon ($\Phi_{\gamma 1}$), the azimuthal angle distribution of the least energetic final photon ($\Phi_{\gamma 2}$), and the invariant mass distribution of the $\gamma\gamma$ pair ($m_{\gamma\gamma}$), presented in Fig. 2. It is interesting to notice that the presence of an NCQED signal changes the behavior of the azimuthal angle distribution of a final photon, while other known examples of new physics cannot produce a similar effect. However, an impressive reduction of the SM background with small effect over the NCQED signal can be achieved by a cut in the invariant mass distribution of the $\gamma\gamma$ pairs. As illustrated in Fig. 2, the invariant mass distribution for the SM background contribution is a decreasing function of the $\gamma\gamma$ invariant mass while the NCQED contribution first increases with the $\gamma\gamma$ invariant mass reaching its maximum value at $m_{\gamma\gamma} \sim 850\,\mathrm{GeV}$ and then decreases. Consequently, in order to enhance the WBF signal for the NCQED $\gamma\gamma\gamma$ and $\gamma\gamma\gamma\gamma$ couplings we imposed the following additional cut in the diphoton invariant mass spectrum:

$$400\,\mathrm{GeV} \ \leq m_{\gamma\gamma} \leq 2500\,\mathrm{GeV}. \tag{11}$$

The results presented in Fig. 2 were obtained using $\sqrt{\hat{s}}$ as the factorization scale in the parton distribution functions, and the renormalization scale (μ_R) used in the evaluation of the QCD coupling constant $[\alpha_\mathrm{S}(\mu_\mathrm{R})]$ was defined such that $\alpha_\mathrm{s}^2(\mu_\mathrm{R}) = \alpha_\mathrm{s}(p_\mathrm{T}^{\mathrm{j}1})\alpha_\mathrm{s}(p_\mathrm{T}^{\mathrm{j}2})$, where $p_\mathrm{T}^{\mathrm{j}1}$ and $p_\mathrm{T}^{\mathrm{j}2}$ are the transverse momenta of the tagging jets.

The evaluation of the SM background (σ_SM) deserves some special care, since it has a large contribution from QCD subprocesses, the size of which depends on the choice of the renormalization scale used in the evaluation of the QCD coupling constant, $\alpha_\mathrm{s}(\mu_\mathrm{R})$, as well as on the factorization scale μ_F used for the parton distribution functions. To estimate the uncertainty associated with these choices, we have reproduced the procedure used in [14], computing σ_SM for two sets of renormalization scales, which we label as $\mu_{\mathrm{R}1,2}(\xi)$, and for several values of μ_F. $\mu_{\mathrm{R}1}(\xi)$ is defined such that $\alpha_\mathrm{s}^2(\mu_{\mathrm{R}1}(\xi)) = \alpha_\mathrm{s}(\xi p_\mathrm{T}^{\mathrm{j}1})\alpha_\mathrm{s}(\xi p t_\mathrm{T}^{\mathrm{j}2})$ where $p_\mathrm{T}^{\mathrm{j}1}$ and $p_\mathrm{T}^{\mathrm{j}2}$ are the transverse momentum of the tagging jets and ξ is a free parameter varied between 0.1 and 10. The second choice of renormalization scale set is $\mu_{\mathrm{R}2}(\xi) = \xi\sqrt{\hat{s}}/2$, with $\sqrt{\hat{s}}$ being the subprocess center-of-mass energy.

From now on our results will be presented assuming a 85% detection efficiency of isolated photons and jet tagging. With this the efficiency for reconstructing the final state $j{+}j{+}\gamma{+}\gamma$ is $(0.85)^4 \approx 52\%$ which is included in our results.

[1] Another advantage of the choice of cuts (9) is the following: if we assume that possible non-commutative quark–quark–photon interactions have an exponential dependence involving the real antisymmetric matrix $C_{\mu\nu}$, like the NCQED lepton–lepton–photon interaction given by $\gamma_\mu f(p_1)\bar{f}(p2):\ \mathrm{i}g\gamma^\mu \exp\left(\frac{\mathrm{i}p_1 C p_2}{2\Lambda^2}\right)$, then the effects of these non-commutative quark–quark–photon interactions are negligible because the set of cuts (9) makes $\exp\left(\frac{\mathrm{i}p_\mathrm{quark} C p_\mathrm{quark}}{2\Lambda^2}\right) \to 1$, allowing us to consider only SM quark–quark–photon interactions in our analysis.

Table 1. Results for $\sigma_{\rm SM}$ for the process (8); see text for details. All results include the effect of the cuts in (9), (10) and (11) as well as photon detection and jet-tagging efficiencies

	$\sigma_{\rm SM}$ (fb)					
	$\mu_{\rm R} = \mu_{\rm R1}(\xi)$			$\mu_{\rm R} = \mu_{\rm R2}(\xi)$		
ξ	$\mu_{\rm F} = \sqrt{\hat{s}}$	$\mu_{\rm F} = p_{\rm min}^{\rm T}$	$\mu_{\rm F} = \sqrt{\hat{s}}/10$	$\mu_{\rm F} = \sqrt{\hat{s}}$	$\mu_{\rm F} = p_{\rm min}^{\rm T}$	$\mu_{\rm F} = \sqrt{\hat{s}}/10$
0.10	3.2	5.3	4.1	1.3	2.2	1.7
0.25	2.2	3.6	2.8	1.1	1.9	1.4
1.00	1.4	2.4	1.9	0.91	1.5	1.2
4.00	1.1	1.8	1.4	0.78	1.3	1.0
10.0	0.94	1.6	1.2	0.71	1.2	0.96

In Table 1 we list $\sigma_{\rm SM}$ for the two sets of renormalization scales and for three values of the factorization scale $\mu_{\rm F} = \sqrt{\hat{s}}, \sqrt{\hat{s}}/10$, and $p_{\rm min}^{\rm T}$, where $p_{\rm min}^{\rm T} = \min(p_{\rm T}^{\rm j1}, p_{\rm T}^{\rm j2})$. As shown in this table, we find that the predicted SM background can change by a factor of ~ 8 depending on the choice of the QCD scales. These results indicate that to obtain meaningful information about the presence of NCQED $\gamma\gamma\gamma$ and $\gamma\gamma\gamma\gamma$ couplings one cannot rely on the theoretical evaluation of the background. Instead one should attempt to extract the value of the SM background from data in a region of phase space where no signal is expected and then extrapolate to the signal region.

In looking for the optimum region of phase space to perform this extrapolation, one must search for kinematic distributions for which
(i) the shape of the distribution is as independent as possible of the choice of QCD parameters. Furthermore, since the electroweak and QCD contributions to the SM backgrounds are of the same order,[2] this requires that
(ii) the shape of both electroweak and QCD contributions are similar.

Several kinematic distributions verify condition (i), for example, the azimuthal angle separation of the two tagging jets which was proposed in [15] to reduce the perturbative QCD uncertainties of the SM background estimation for invisible Higgs searches at LHC. However, the totally different shape of the electroweak background in the present case renders this distribution useless.

We found that the best sensitivity is obtained by using the $\gamma\gamma$ invariant mass. As can be seen in Fig. 2, the shape of the SM distribution is quite independent of the choice of the QCD parameters. As a consequence most of the QCD uncertainties cancel in the ratio

$$R(\xi) = \frac{\sigma(400\ \text{GeV}\ < m_{\gamma\gamma} < 2500\,\text{GeV}\ )}{\sigma(100\,\text{GeV}\ < m_{\gamma\gamma} < 400\,\text{GeV}\ )}\ . \qquad (12)$$

This fact is illustrated in Fig. 3, where we plot the value of the ratio $R(\xi)$ for different values of the renormalization and factorization scales. The ratio R is almost invariant under changes of the renormalization scale, showing a maximum variation of the order of $\pm 6\%$ for a fixed value of the factorization scale. On the other hand, the uncertainty

[2] The electroweak contribution to the total SM background is approximately 25% for $\mu_{\rm R1}(\xi = 1)$ and $\mu_{\rm F} = \sqrt{\hat{s}}$.

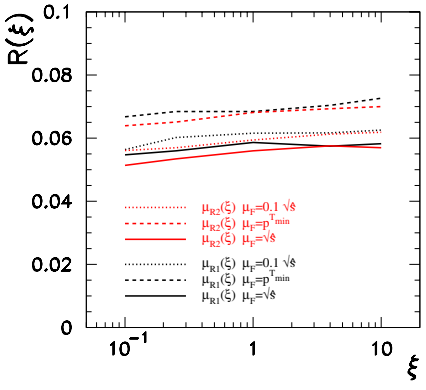

Fig. 3. Ratio $R(\xi)$ defined in (12) for the process $pp \to \gamma\gamma jj$ at LHC

on the factorization scale leads to a maximum variation of 12% in the background estimation. We have also verified that different choices for the structure functions do not affect these results.

Thus the strategy here proposed is simple: the experiments should measure the number of events in the $\gamma\gamma$ invariant mass window $100 < m_{\gamma\gamma} < 400\,\text{GeV}$ and extrapolate the results for higher invariant masses using perturbative QCD. According to the results described above we can conservatively assign a maximum "QCD" uncertainty ($\text{QCD}_{\rm unc}$) of $\pm 15\%$ to this extrapolation.

In order to estimate the attainable sensitivity to NCQED we assume that the observed number of events is compatible with the expectations for $\mu_{\rm R1}(\xi = 1)$ and $\mu_{\rm F} = \sqrt{\hat{s}}$, so the observed number of events in the signal region coincides with the estimated number of background events obtained from the extrapolation of the observed number of events in the region where no signal is expected; for this choice the number of expected background events is $N_{\rm SM} = \sigma_{\rm SM}\mathcal{L}$ where $\mathcal{L}$ stands for the integrated luminosity. For an integrated luminosity of $100\,\text{fb}^{-1}$ for LHC, this corresponds to $N_{\rm back} = 143$. Moreover, we have added in quadrature the statistical error and the QCD uncertainty associated with the backgrounds. Therefore, the 95% C.L. limits on Λ can be obtained from the condition

$$N_{\rm NCQED} = \mathcal{L} \times \sigma_{\rm NCQED} \leq 1.95\sqrt{N_{\rm SM} + (N_{\rm SM} \times \text{QCD}_{\rm unc})^2}\ , \qquad (13)$$

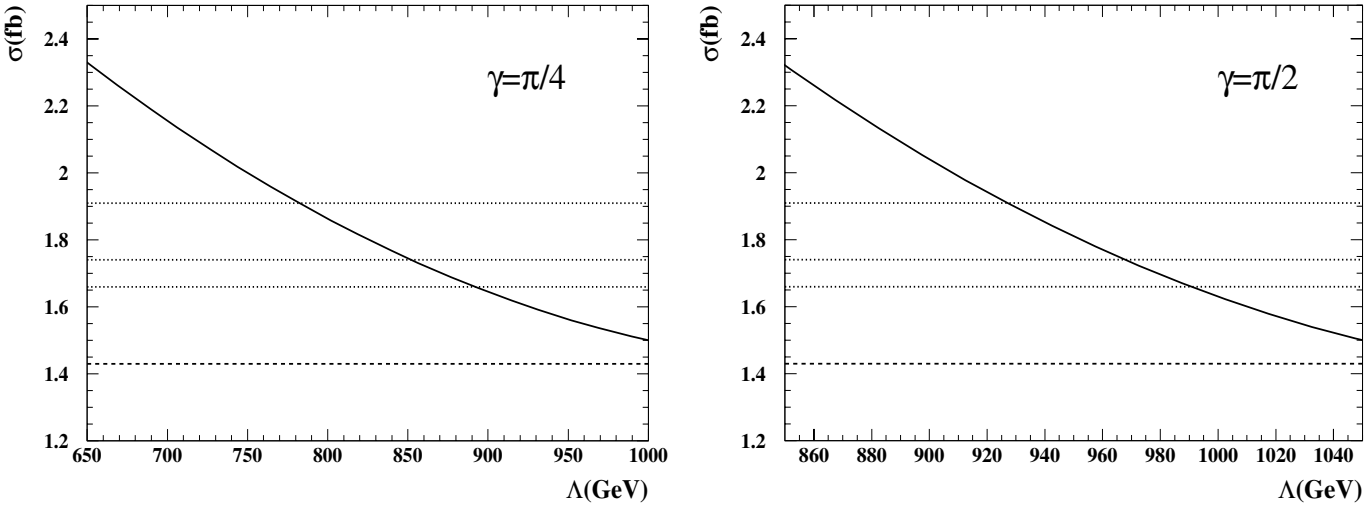

Fig. 4. Cross section results including the effect of the cuts in (9), (10) and (11) as well as photon detection and jet-tagging efficiencies. The solid line is the cross section including space-space NCQED effects, the dashed line is the SM cross section, and the upper (medium) [lower] dotted line represents the 95% C.L. upper limit for an QCD uncertainty of 15% (7.5%) [0]

Table 2. 95% C.L. maximum cross section and number of events deviation due to the NCQED contribution

$\mathrm{QCD_{unc}}$	σ_{NCQED} (fb)	N_{NCQED}
0	0.23	23
7.5%	0.31	31
15%	0.48	48

where N_{NCQED} (σ_{NCQED}) is the maximum number of events (cross section) deviation due to the NCQED contribution, so $N_{\mathrm{observed}} = N_{\mathrm{SM}} \pm N_{\mathrm{NCQED}}$. Once we have $\mathcal{L} = 100\,\mathrm{fb}^{-1}$ and $N_{\mathrm{back}} = 143$, (13) turns out to be

$$\sigma_{\mathrm{NCQED}}(\mathrm{fb}) \leq 0.0195 \times \sqrt{143 + (143 \times \mathrm{QCD_{unc}})^2}\ . \quad (14)$$

For the sake of completeness we show the results on the expected sensitivity using purely statistical errors and for two values of $\mathrm{QCD_{unc}}$: our most conservative estimate [15%], and a possible reduced uncertainty (7.5%), which could be attainable provided NLO QCD calculations are available. Therefore the NCQED deviation should not be greater than the values presented in Table 2.

Once we have fixed ϕ by settling $\beta = \pi/2$ in (7), the antisymmetric matrix gets parameterized by two angles: the angle α related to the space-time non-commutativity, and the angle γ related to the space-space non-commutativity. Therefore, in order to perform our analysis we consider two cases:
(i) the space-space non-commutativity, where the elements C_{0i} $(i = 1, 2, 3)$ in (7) are assumed to be 0, and the angle γ is assumed to be either 0, $\pi/4$ or $\pi/2$;
(ii) the space-time non-commutativity, where the elements C_{ij} $(i, j = 1, 2, 3)$ in (7) are assumed to be 0, and the angle α is assumed to be either 0, $\pi/4$ or $\pi/2$.

In order to determine which case of NCQED is being observed, one can use the azimuthal angle distribution of a final photon. As illustrated in Fig. 2, the azimuthal angle distribution of either the most or the least energetic final photon for the SM background contribution is a flat function in the range $|\Phi_\gamma| < \frac{\pi}{2}$, while for the space-time (space-space) non-commutativity signal contribution, the distribution is increased for $|\Phi_\gamma| \to \frac{\pi}{2}(0)$.[3]

The evaluation of the cross section of the reaction (8), including the effect of the cuts in (9), (10) and (11) as well as photon detection and jet-tagging efficiencies, is now done including the effect of the diagrams in Fig. 1, for the cases (i) and (ii) described above.

The results for the space-space non-commutativity, case (i), are presented in Fig. 4, for $\gamma = \pi/4$, and $\pi/2$. No limits on Λ could be obtained for $\gamma = 0$. Our analysis shows a better sensitivity for the angle $\gamma = \pi/2$, allowing us to impose a lower limit on the NCQED scale of $\Lambda \gtrsim 990$ GeV if the QCD uncertainty discussed above is not considered. The limit changes to $\Lambda \gtrsim 930$ (960) GeV for a QCD uncertainty of 15% (7.5%). For $\gamma = \pi/4$, the lower limit on the NCQED scale is $\Lambda \gtrsim 780$ (850) [900] GeV for a QCD uncertainty of 15% (7.5%) [0%].

On the other hand, the results for the space-time non-commutativity, case (ii), are presented in Fig. 5, for $\alpha = 0$, $\pi/4$, and $\pi/2$, respectively. Our analysis shows a better sensitivity for the angle $\alpha = 0$, allowing us to impose a lower limit on the NCQED scale of $\Lambda \gtrsim 1320$ GeV if the QCD uncertainty discussed above is not considered. The limit changes to $\Lambda \gtrsim 1290$ (1230) GeV for a QCD uncertainty of 15% (7.5%). For $\alpha = \pi/4$, the lower limit on the NCQED scale is $\Lambda \gtrsim 1130$ (1190) [1230] GeV for a QCD uncertainty of 15% (7.5%) [0%] and for $\alpha = 0$, the lower limit on the NCQED scale is $\Lambda \gtrsim 920$ (960) [990] GeV for a QCD uncertainty of 15% (7.5%) [0%].

[3] We have checked that this angular behavior is preserved for $\Lambda \simeq 1$ TeV after the inclusion of the cut (11) in our evaluations.

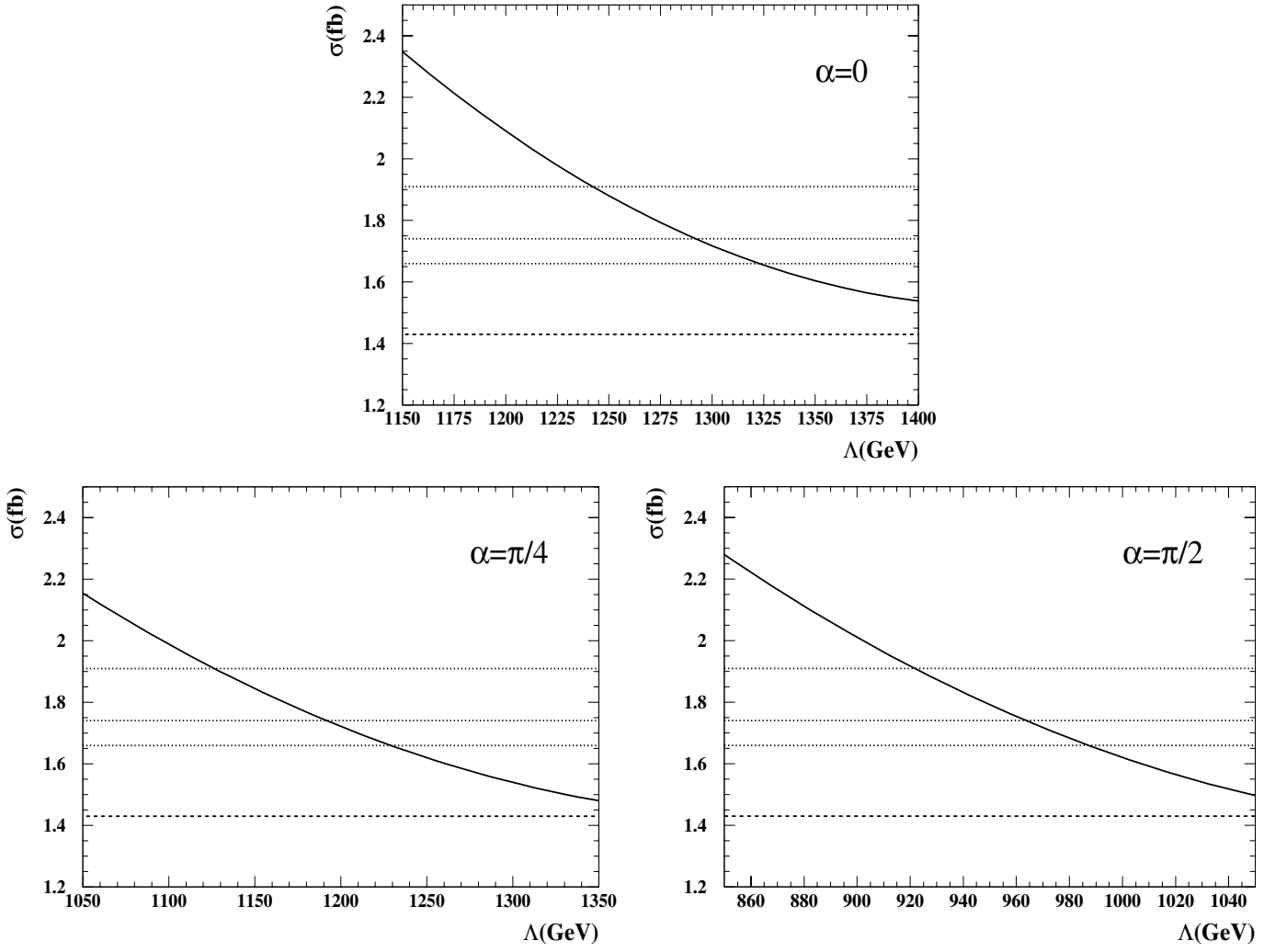

Fig. 5. Cross section results including the effect of the cuts in (9), (10) and (11) as well as photon detection and jet-tagging efficiencies. The solid line is the cross section including space-time NCQED effects, the dashed line is the SM cross section, and the upper (medium) [lower] dotted line represents the 95% C.L. upper limit for an QCD uncertainty of 15% (7.5%) [0]

4 Conclusions

In this work we investigated the potential for LHC to probe the photonic 3- and 4-point functions that appears in NCQED through an analysis of the process (8). Even though we assumed that the quark–quark–photon interactions make up part of the SM background due to our choice of kinematical cuts, this process is sensitive to space-space as well as for space-time non-commutativity. Our main results are presented in Figs. 4 and 5 where the space-space and space-time NCQED effects are observed.

For the space-space non-commutativity, our study shows a better sensitivity for the angle $\gamma = \pi/2$, allowing us to impose a lower limit on the NCQED scale Λ in the range $930\,\text{GeV} \leq \Lambda \leq 990\,\text{GeV}$, depending on the perturbative QCD uncertainties considered. Regarding the space-time non-commutativity, the process is more sensitive for the angle $\alpha = 0$, where a lower limit on the NCQED scale Λ in the range $1230\,\text{GeV} \leq \Lambda \leq 1320\,\text{GeV}$, depending on the perturbative QCD uncertainties considered, could be imposed.

Therefore, this work shows that LHC may be a good place to test NCQED via the study of the process (8). We have shown that LHC is able to probe both space-space and space-time non-commutativity. A better sensitivity is expected for the space-time non-commutativity, where the NCQED scale Λ can be tested up to $\Lambda \sim 1.25\,\text{TeV}$.

Acknowledgements. The authors would like to thank R.F. Ribeiro for useful discussions. S.M. Lietti thanks for the hospitality received at UFPb during the early stage of this work. This work was supported by Conselho Nacional de Desenvolvimento Científico e Tecnológico (CNPq), and by Fundação de Amparo à Pesquisa do Estado de São Paulo (FAPESP).

References

1. H.S. Snyder, Phys. Rev. D **71**, 38 (1947)
2. A. Connes, M.R. Douglas, A. Schwarz, J. High Energy Phys. **9802**, 003 (1998)

3. N. Seiberg, E. Witten, J. High Energy Phys. **9909**, 032 (1999)
4. N. Arkani-Hamed, S. Dimopoulos, G. Dvali, Phys. Lett. B **429**, 263 (1998); L. Randal, R. Sundrum, Phys. Rev. Lett. **83**, 3370 (1999)
5. J.L. Hewett, F.J. Petriello, T.G. Rizzo, Phys. Rev. D **64**, 075012 (2001)
6. T. Rizzo, Int. J. Mod. Phys. A **18**, 2797 (2003); S. Godfrey, M.A. Doncheski, Phys. Rev. D **65**, 015005 (2002); A. Anisimov, T. Banks, M. Dine, M. Graesser, Phys. Rev. D **65**, 085032 (2002); H. Grosse, Y. Liao, Phys. Rev. D **64**, 115007 (2001); S-W Baek, D.K. Ghosh, X-G He, W.Y.P. Hwang, Phys. Rev. D **64**, 056001 (2001); S. Godfrey, M.A. Doncheski, hep-ph/0111147; N. Mahajan, hep-ph/0110148
7. P. Mathews, Phys. Rev. D **63**, 075007 (2001)
8. For an excellent review of the phenomenology of NCQED, see I. Hinchliffe, N. Kersting, hep-ph/0205040
9. A. Armoni, Nucl. Phys. B **593**, 229 (2001); M. Chaichian, P. Presnajder, M.M. Sheikh-Jabbari, A. Tureanu, Eur. Phys. J. C **29**, 413 (2003)
10. X. Calmet, B. Jurco, P. Schupp, J. Wess, M. Wohlgenannt, Eur. Phys. J. C **23**, 363 (2002)
11. W. Behr, N.G. Deshpande, G. Duplancic, P. Schupp, J. Trampetic, J. Wess, Eur. Phys. J. C **29**, 441 (2003); E.O. Iltan, Phys. Rev. D **66**, 034011 (2002)
12. T. Stelzer, W.F. Long, Comput. Phys. Commun. **81**, 357 (1994)
13. H. Murayama, I. Watanabe, K. Hagiwara, KEK report 91-11 (unpublished)
14. O.J.P. Éboli, M.C. Gonzalez-Garcia, S.M. Lietti, hep-ph/0310141
15. O.J. Éboli, D. Zeppenfeld, Phys. Lett. B **495**, 147 (2000)